J|A|C|S
ARTICLES
Published on Web 04/13/2007

Helical Pores Self-Assembled from Homochiral Dendritic Dipeptides Based on L-Tyr and Nonpolar α-Amino Acids

Virgil Percec,*,† Andrés E. Dulcey,† Mihai Peterca,†,‡ Peter Adelman,† Ritika Samant,† Venkatachalapathy S. K. Balagurusamy,‡ and Paul A. Heiney‡

Contribution from the Roy and Diana Vagelos Laboratories, Department of Chemistry, University of Pennsylvania, Philadelphia, Pennsylvania 19104-6323, and Department of Physics and Astronomy, University of Pennsylvania, Philadelphia, Pennsylvania 19104-6396

Received February 14, 2007; E-mail: percec@sas.upenn.edu

Abstract: The synthesis of dendritic dipeptides (4-3,4-3,5)12G2-CH_2-Boc-L-Tyr-X-OMe where X = Gly, L-Val, L-Leu, L-Ile, L-Phe, and L-Pro is reported. Their self-assembly in bulk and in solution and the structural and retrostructural analysis of their periodic assemblies were compared to those of the previously reported and currently reinvestigated dendritic dipeptides with X = L-Ala. All dendritic dipeptides containing as X nonpolar α-amino acids self-assemble into helical porous columns. The substituent of X programs the structure of the helical pore and the resulting periodic array, in spite of the fact that its molar mass represents only between 0.05 and 4.77% from the molar mass of the dendritic dipeptide. In addition to the various 2-D columnar lattices, the dendritic dipeptides based on L-Ala, L-Leu, and L-Phe self-organize into 3-D hexagonal columnar crystals while those based on L-Val and L-Ile into an unknown columnar crystal. The principles via which the aliphatic and aromatic substituents of X program the structure of the helical pores indicate synthetic pathways to helical pores with bioinspired functions based on artificial nonpolar α-amino acids.

Introduction

Natural porous proteins function as viral helical coats,[1] transmembrane channels responsible for ion regulation and transport, molecular recognition and response, and energy transduction,[2] antibiotics,[3] antimicrobials,[4] and toxins.[5] Remodeled porous proteins are used for reversible encapsulation of molecules[6] and in stochastic sensing.[7] Integral membrane proteins, including those functioning as transmembrane channels, exist in very low natural abundance, and since they form three-dimensional functional structures only in the membrane environment, their crystallization had limited success. Therefore, the molecular details of their structure and function are not well understood.[2,3] Simple synthetic assemblies that mimic the structure and function of transmembrane channels are expected to contribute to the understanding of the structure and function of the more complex natural proteins. Strategies for the synthesis and assembly of porous or tubular supramolecular structures have been elaborated.[8] Natural porous proteins are stable in the fluid membrane environment and in the solid state. However, with few exceptions,[9] porous protein mimics do not assemble into periodically ordered structures that are stable in solution and in the solid state. This behavior limits their structural analysis by combinations of solution and solid-state complementary techniques. Recently, our laboratory elaborated a new strategy to helical porous protein mimics that is based on the self-assembly of amphiphilic dendritic dipeptides.[10] The internal structure and stability of the porous structure self-assembled from dendritic dipeptides are programmed by the stereochem-

† Department of Chemistry.
‡ Department of Physics and Astronomy.

(1) (a) Klug, A. *Angew. Chem., Int. Ed. Engl.* **1983**, *22*, 565−582. (b) Klug, A. *Philos. Trans. R. Soc. London, Ser. B* **1999**, *354*, 531−535.
(2) (a) MacKinnon, *R. Angew. Chem., Int. Ed.* **2004**, *43*, 4265−4277. (b) Agre, P. *Angew. Chem., Int. Ed.* **2004**, *43*, 4278−4290.
(3) Wallace, B. A. *Biophys. J.* **1986**, *49*, 295−306.
(4) (a) Zasloff, M. *Nature* **2002**, *415*, 389−395. (b) White, S. H.; Winley, W. C.; Selsted, M. E. *Curr. Opin. Struct. Biol.* **1995**, *5*, 521−527.
(5) (a) Gouaux, E. *J. Struct. Biol.* **1998**, *121*, 110−122. (b) Gouaux, E. *Curr. Opin. Struct. Biol.* **1997**, *7*, 566−573.
(6) Bayley, H.; Cremer, P. S. *Nature* **2001**, *413*, 226−230.
(7) (a) Ishii, D.; Kinbara, K.; Ishida, Y.; Ishii, N.; Okochi, M.; Yohda, M.; Aida, T. *Nature* **2003**, *423*, 628−632. (b) Douglas, T.; Young, M. *Science* **2006**, *312*, 873−875.
(8) (a) Nolte, R. J. M.; van Beijnen, A. J. M.; Neevel, J. G.; Zwikker, J. W.; Verkley, A. J.; Drenth, W. *Isr. J. Chem.* **1984**, *24*, 297−301. (b) Jullien, L.; Lehn, J.-M. *Tetrahedron Lett.* **1988**, *29*, 3803−3806. (c) Cross, G. G.; Fyles, T. M.; James, T. D.; Zojaji, M. *Synlett* **1993**, *7*, 449−460. (d) Gokel, G. W.; Ferdani, R.; Liu, J.; Pajewski, R.; Shabany, H.; Uetrecht, P. *Chem.−Eur. J.* **2001**, *7*, 33−39. (e) Bong, D. T.; Clark, T. D.; Granja, J. R.; Ghadiri, M. R. *Angew. Chem., Int. Ed.* **2001**, *40*, 988−1011. (f) Sakai, N.; Mareda, J.; Matile, S. *Acc. Chem. Res.* **2005**, *38*, 79−87. (g) Rosselli, S.; Ramminger, A.-D.; Wagner, T.; Silier, B.; Wiegand, S.; Häussler, W.; Lieser, G.; Scheumann, V.; Höger, S. *Angew. Chem., Int. Ed.* **2001**, *40*, 3138−3141. (h) Hill, D. J.; Mio, M. J.; Prince, R. B.; Hughes, T. S.; Moore, J. S. *Chem. Rev.* **2001**, *101*, 3893−4012. (i) Fenniri, H.; Deng, B.-L.; Ribbe, A. E. *J. Am. Chem. Soc.* **2002**, *124*, 11064−11072. (j) Hecht, S.; Khan, A. *Angew. Chem., Int. Ed.* **2003**, *42*, 6021−6024. (k) Couet, J.; Jeyaprakash, J. D.; Samuel, S.; Kopyshev, A.; Santer, S.; Biesalski, M. *Angew. Chem., Int. Ed.* **2005**, *44*, 3297−3301.
(9) (a) Ghadiri, M. R.; Granja, J. R.; Milligan, R. A.; McRee, D. E.; Khazanovich, N. *Nature* **1993**, *366*, 324−327. (b) Petitjean, A.; Cuccia, L. A.; Lehn, J.-M.; Nierengarten, H.; Schmutz, M. *Angew. Chem., Int. Ed.* **2002**, *41*, 1195−1198. (c) Ohkita, M.; Lehn, J.-M.; Baum, G.; Fenske, D. *Chem.−Eur. J.* **1999**, *5*, 3471−3481. (d) Schmitt, J.-L.; Stadler, A.-M.; Kyritsakas, N.; Lehn, J.-M. *Helv. Chim. Acta* **2003**, *86*, 1598−1624. (e) Schmitt, J.-L.; Lehn, J.-M. *Helv. Chim. Acta* **2003**, *86*, 3417−3426.
(10) (a) Percec, V.; Dulcey, A. E.; Balagurusamy, V. S. K.; Miura, Y.; Smidrkal, J.; Peterca, M.; Nummelin, S.; Edlund, U.; Hudson, S. D.; Heiney, P. A.; Duan, H.; Magonov, S. N.; Vinogradov, S. A. *Nature* **2004**, *430*, 764−768. (b) Rouhi, M. *Chem. Eng. News* **2004**, *82* (33), 4. (c) Borman, S. *Chem. Eng. News* **2004**, *82* (51), 53−61.

 10.1021/ja071088k CCC: $37.00

Scheme 1. Synthesis of Dendritic Dipeptides (4-3,4-3,5)12G2-CH_2-Boc-L-Tyr-X-OMe, X = Gly (**14**), L-Val (**15**), L-Leu (**16**), L-Ile (**17**), L-Phe (**18**), L-Pro (**19**)

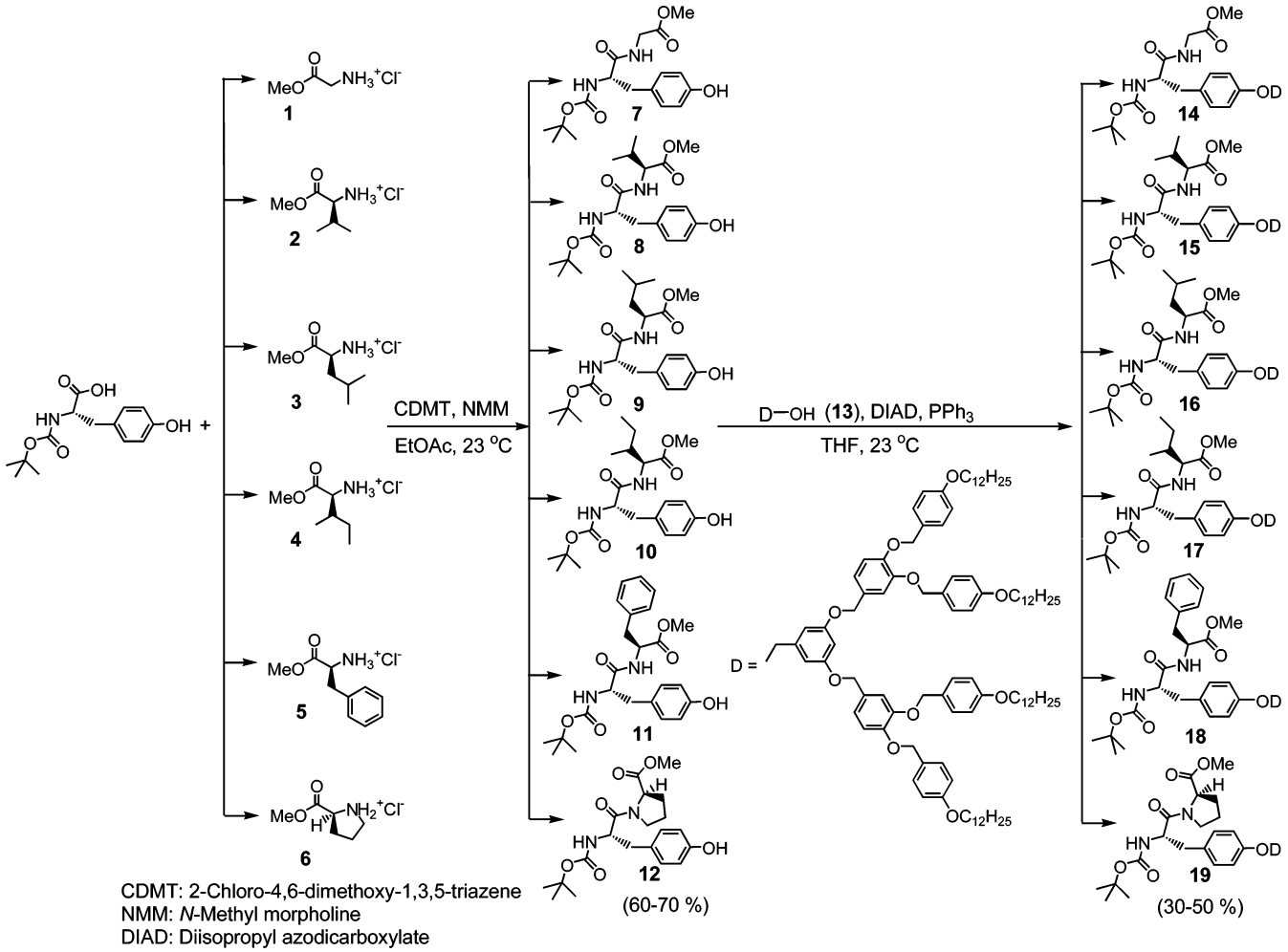

istry[11a] and protective groups[11b] of the dipeptide, by the number of methylenic units from the alkyl groups of the dendron,[11c] and by the primary structure of the dendron attached to the dipeptide.[11d,e] These experiments provided some of the molecular principles required to program the self-assembly of helical pores from dendritic dipeptides. This cooperative self-assembly process involves allosteric regulation.[11,12] In all previous studies the dendritic dipeptide was constructed from Boc-Tyr-Ala-OMe dipeptide containing various combinations of Tyr and Ala stereochemistry,[10,11a] different protective groups,[11b] and dendron architectures.[11c−e] In order to assess the scope, limitations, and generality of this self-assembly strategy, the synthesis, self-assembly, structural and retrostructural analysis of the dendritic dipeptides (4-3,4-3,5)12G2-CH_2-Boc-L-Tyr-X-OMe, in which X are all nonpolar α-amino acids Gly, L-Val, L-Leu, L-Ile, L-Phe, and L-Pro, were investigated. The results of this study are reported and compared with that of the dendritic dipeptide with X = L-Ala which was studied previously[10,11] and was reinvestigated here.

Results and Discussion

Synthesis of Dendritic Dipeptides (4-3,4-3,5)12G2-CH_2-Boc-L-Tyr-X-OMe with X = Gly, L-Val, L-Leu, L-Ile, L-Phe, and L-Pro. The dipeptides Boc-L-Tyr-Gly-OMe (**7**), Boc-L-Tyr-L-Val-OMe (**8**), Boc-L-Tyr-L-Leu-OMe (**9**), Boc-L-Tyr-L-Ile-OMe (**10**), Boc-L-Tyr-L-Phe-OMe (**11**), and Boc-L-Tyr-L-Pro-OMe (**12**) were synthesized from Boc *N*-protected L-Tyr with the hydrochloride of the methyl ester of the nonpolar α-amino acids Gly (**1**), L-Val (**2**), L-Leu (**3**), L-Ile (**4**), L-Phe (**5**), and L-Pro (**6**) in the presence of 2-chloro-4,5-dimethoxy-1,3,5-triazene (CDMT)[10,13]/*N*-methylmorpholine (NMM) in EtOAc at 23 °C (Scheme 1). All dipeptides were obtained in 60 to 70% yield after purification by column chromatography (SiO_2/gradient 2−4% MeOH in $CHCl_3$). The dendritic dipeptides (4-3,4-3,5)12G2-CH_2-Boc-L-Tyr-X-OMe (**14**−**19**) were synthesized by Mitsunobu etherification[14] of the benzyl alcohol group of the second generation dendritic alcohol (4-3,4-3,5)12G2-CH_2-

(11) (a) Percec, V.; Dulcey, A. E.; Peterca, M.; Ilies, M.; Ladislaw, J.; Rosen, B. M.; Edlund, U.; Heiney, P. A. *Angew. Chem., Int. Ed.* **2005**, *44*, 6516−6521. (b) Percec, V.; Dulcey, A. E.; Peterca, M.; Ilies, M.; Sienkowska, M. J.; Heiney, P. A. *J. Am. Chem. Soc.* **2005**, *127*, 17902−17909. (c) Percec, V.; Dulcey, A. E.; Peterca, M.; Ilies, M.; Nummelin, S.; Sienkowska, M. J.; Heiney, P. A. *Proc. Natl. Acad. Sci. U.S.A.* **2006**, *103*, 2518−2523. (d) Percec, V.; Dulcey, A. E.; Peterca, M.; Ilies, M.; Miura, Y.; Edlund, U.; Heiney, P. A. *Aust. J. Chem.* **2005**, *58*, 472−482. (e) Peterca, M.; Percec, V.; Dulcey, A. E.; Nummelin, S.; Korey, S.; Ilies, M.; Heiney, P. A. *J. Am. Chem. Soc.* **2006**, *128*, 6713−6720.

(12) (a) Monod, J.; Changeux, J.-P.; Jacob, F. *J. Mol. Biol.* **1963**, *6*, 306−329. (b) Perutz, M. *Mechanisms of Cooperativity and Allosteric Regulation in Proteins*; Cambridge University Press: Cambridge, U.K., 1990. (c) Evans, P. R. *Curr. Opin. Struct. Biol.* **1991**, *1*, 773−779.

(13) Kronin, J. S.; Ginah, F. O.; Murray, A. R.; Copp, J. D. *Synth. Commun.* **1996**, *26*, 3491−3494.

(14) Mitsunobu, O. *Synthesis* **1981**, 1−28.

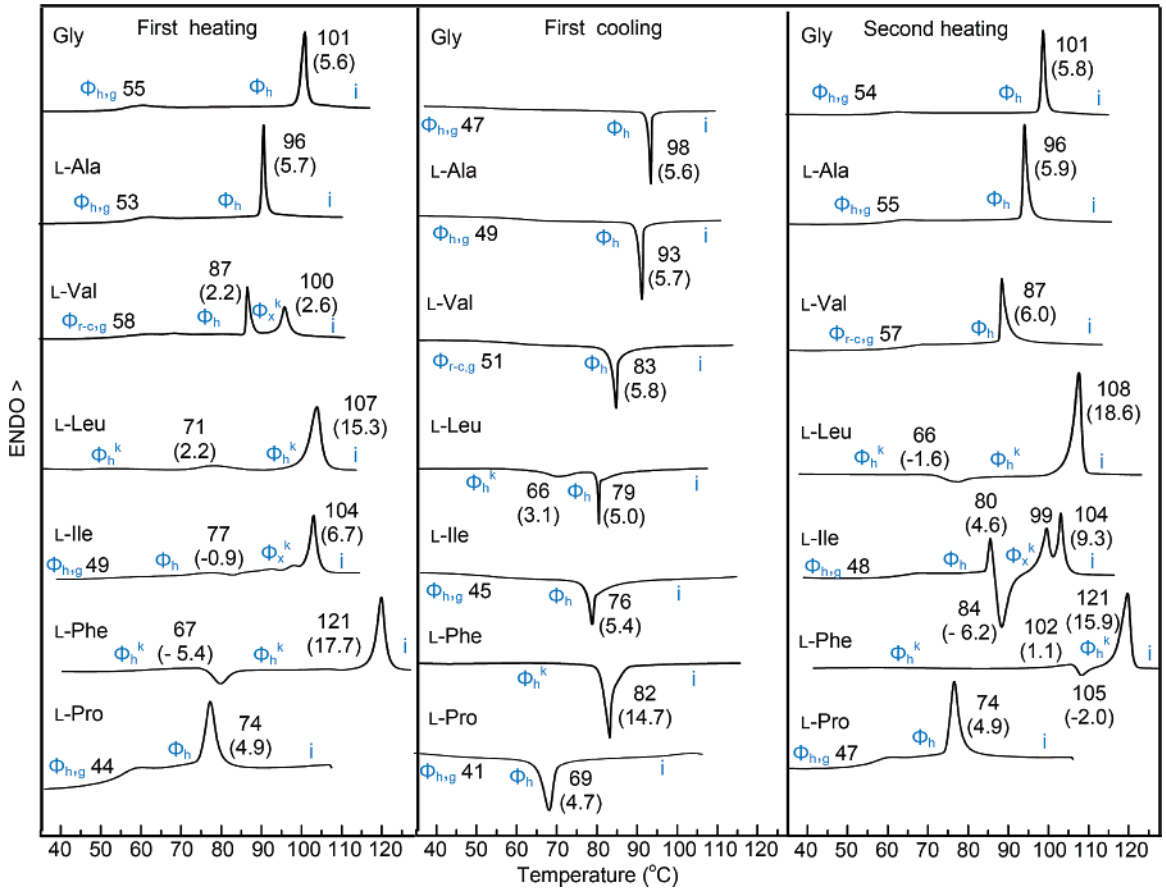

Figure 1. DSC traces of (4-3,4-3,5)12G2-CH_2-Boc-L-Tyr-X-OMe. The structure of α-amino acid X from dipeptide, the phases, the transition temperatures (in °C), and the corresponding enthalpy changes (in kcal/mol, in brackets) are indicated; *g* = glassy; Φ_h, hexagonal columnar liquid crystal phase; Φ_h^k, hexagonal columnar crystal phase; Φ_x^k, unknown columnar crystal phase; Φ_{r-c}, centered rectangular columnar liquid crystal phase. Φ_h^k phases separated by endo or exo peaks exhibit different degrees of crystallinity and/or column and pore diameter.

OH[15] with the hydroxyphenyl group of the dipeptides **7**−**12**, respectively. All dendritic dipeptides, with higher purities than 99% (HPLC), were obtained in 30 to 50% yield after purification by flash column chromatography (SiO_2/gradient 2−4% MeOH in $CHCl_3$). Additional details for the synthesis and structural analysis of the dipeptides and dendritic dipeptides by a combination of 500 MHz ^{1}H NMR, 125 MHz ^{13}C NMR, HPLC, MALDI-TOF, and elemental analysis are available in the Supporting Information and in its Tables ST1 and ST2. The CH_2Cl_2 solution of pure dendritic dipeptides was precipitated in CH_3OH, and the compounds were dried before being subjected to structural analysis.

Structural Analysis in the Solid State by Differential Scanning Calorimetry and Small-Angle X-ray Diffraction. The as-prepared samples of all dendritic dipeptides are already self-assembled into porous supramolecular columns that are self-organized into various periodic columnar arrays. The structural analysis of these periodic arrays was performed by a combination of differential scanning calorimetry (DSC) and powder small-angle X-ray diffraction (XRD) experiments. Figure 1 illustrates the first heating and cooling and the second heating scans of all (4-3,4-3,5)12G2-CH_2-Boc-L-Tyr-X-OMe. The structure of the second α-amino acid from the dipeptide, X, is marked on the left side of each DSC scan. The phase transitions of the periodic arrays and their enthalpy changes were determined by DSC and are summarized in Table 1. Their structure was assigned by XRD. For comparison, the DSC of (4-3,4-3,5)12G2-CH_2-Boc-L-Tyr-L-Ala-OMe is also included in Figure 1.

A brief inspection of the data from Figure 1 reveals that the structure of the substituent of the second α-amino acid from the dipeptide determines the structure and the stability of the periodic arrays assembled from dendritic dipeptides. This is a remarkable result when we consider that the substituent of the second α-amino acid contributes only 0.05% for Gly, 0.8% for L-Ala, 2.31% for L-Val, 3.04% for L-Leu and L-Ile, 4.77% for L-Phe, and 2.26% for L-Pro from the overall molecular mass of the dendritic dipeptide. Moreover, based on the order of the periodic array self-organized from the supramolecular columns, the structure of the substituent of the second α-amino acid from the dipeptide divides them in four groups. (1) Dendritic dipeptides that produce only 2-D hexagonal columnar (Φ_h) liquid crystalline periodic arrays. This group comprises dipeptides that contain as the second α-amino acid Gly, L-Ala, and L-Pro. (2) Dendritic dipeptides that generate a biphasic mixture made out of the Φ_h and an unknown yet columnar crystal phase (Φ_x^k). Only the dipeptide containing L-Val exhibits this behavior in the first heating scan. In subsequent heating and cooling scans this dendritic dipeptide behaves similarly to group (1). (3) Dendritic dipeptides that display a hexagonal columnar crystal phase (Φ_h^k) or the Φ_x^k and a monotropic Φ_h phase. This group

(15) (a) Percec, V.; Cho, W.-D.; Ungar, G.; Yeardley, D. J. P. *J. Am. Chem. Soc.* **2001**, *123*, 1302−1315. (b) Percec, V.; Mitchell, C. M.; Cho, W.-D.; Uchida, S.; Glodde, M.; Ungar, G.; Zeng, X.; Liu, Y.; Balagurusamy, V. S. K.; Heiney, P. A. *J. Am. Chem. Soc.* **2004**, *126*, 6078−6094.

Table 1. Thermal Transitions of (4-3,4-3,5)12G2-CH_2-Boc-L-Tyr-X-OMe

X	thermal transitions (°C) and the corresponding enthalpy changes[a] (kcal/mol)	
	heating	cooling
Gly	$\Phi_{h,g}$[b] 55 Φ_h 101 (5.6) i[c] $\Phi_{h,g}$ 54 Φ_h 101 (5.8) i	i 98 (5.6) Φ_h 47 $\Phi_{h,g}$
L-Ala	$\Phi_{h,g}$ 53 Φ_h 96 (5.7) i $\Phi_{h,g}$ 55 Φ_h 96 (5.9) i [90 °C, 180 min] Φ_h^k[d] 105 (13.1)	i 93 (5.7) Φ_h 49 $\Phi_{h,g}$
L-Val	$\Phi_{r-c,g}$[e] 58 Φ_h 87 (2.2) Φ_x^k 100 (2.6) i $\Phi_{r-c,g}$ 57 Φ_h 87 (6.0) i [80 °C, 40 min] Φ_x^k[f] 99 (12.8)	i 83 (5.8) Φ_h 51 $\Phi_{r-c,g}$
L-Leu	Φ_h^k 71 (2.2) Φ_h^k 107 (15.3) i Φ_h^k 66 (−1.6) Φ_h^k 108 (18.6) i [90 °C, 30 min] Φ_x^k 108 (17.5)	i 79 (5.0) Φ_h 66 (3.1) Φ_h^k
L-Ile	$\Phi_{h,g}$ 49 Φ_h 77 (−0.9) Φ_x^k 104 (6.7) i $\Phi_{h,g}$ 48 Φ_h 80 (4.6) 84 (−6.2) Φ_x^k 99 + 104 (9.3) i [90 °C, 30 min] Φ_x^k 104 (12.9)	i 76 (5.4) Φ_h 45 $\Phi_{h,g}$
L-Phe	Φ_h^k 67 (−5.4) Φ_h^k 121 (17.7) i Φ_h^k 102 (1.1) 105 (−2.0) Φ_h^k 121 (15.9) i [110 °C, 30 min] Φ_h^k 120 (16.7)	i 82 (14.7) Φ_h^k
L-Pro	$\Phi_{h,g}$ 44 Φ_h 74 (4.9) i $\Phi_{h,g}$ 47 Φ_h 74 (4.9) i	i 69 (4.7) Φ_h 41 $\Phi_{h,g}$

[a] First line: data from the first heating and cooling scans. Second line: data from the second heating (after the first cooling). Third line: data from the first heating after annealing at the temperature and for the time indicated in brackets before the transition. [b] Φ_h, hexagonal columnar phase; g, glassy. [c] i, isotropic. [d] Φ_h^k, hexagonal columnar crystal phase. [e] Φ_{r-c}, centered rectangular columnar phase. [f] Φ_x^k, unknown columnar crystal phase.

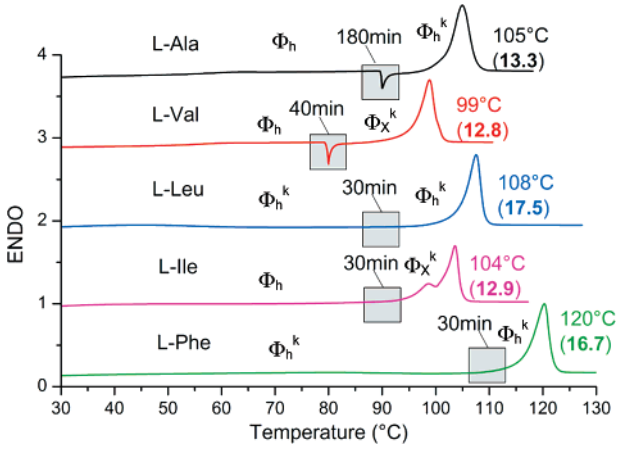

Figure 2. Heating DSC scans of (4-3,4-3,5)12G2-CH_2-Boc-L-Tyr-X-OMe after the sample was annealed at the temperature and for the time indicated. The gray squares indicate the annealing period and temperature. The enthalpy associated with the isotropisation transition increased as compared with the as-prepared samples (Figure 1). The structure of α-amino acid X of the dipeptide is indicated. Φ_h, hexagonal columnar liquid crystal phase; Φ_h^k, hexagonal columnar crystal phase; Φ_x^k, unknown columnar crystal phase.

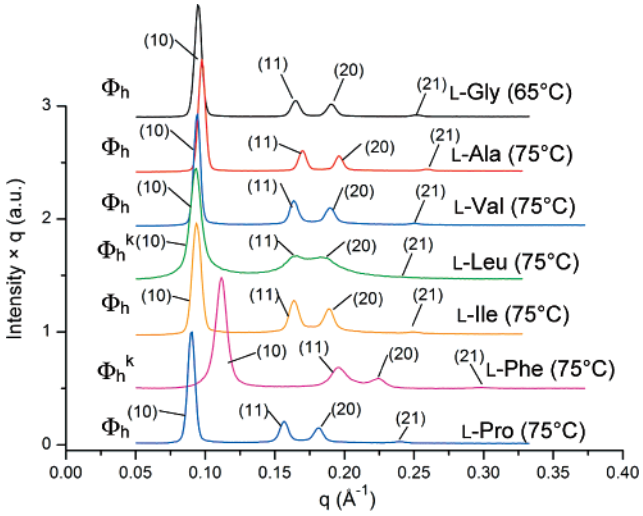

Figure 3. Stack of small-angle powder XRD of (4-3,4-3,5)12G2-CH_2-Boc-L-Tyr-X-OMe in various hexagonal columnar lattices. The structure of α-aminoacid X from dipeptide, the temperatures, the lattices, and the assignment of *d*-spacings are indicated. Φ_h, hexagonal columnar liquid crystal phase; Φ_h^k, hexagonal columnar crystal phase.

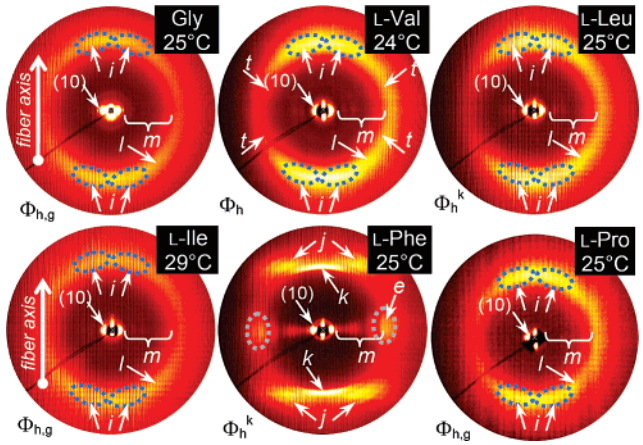

Figure 4. Wide-angle XRD of oriented fibers of (4-3,4-3,5)12G2-CH_2-Boc-L-Tyr-X-OMe in various columnar hexagonal phases. The structure of α-amino acid X from dipeptide, recording temperature, and phase are indicated. The nomenclature of phases is identical to that in Figure 1. *i*, 4.6 Å short-range helical feature; (10) peak of the Φ_h phase; *m*, high order (*hk*0) reflections of the $\Phi_{h,g}$ and Φ_h^k phases; *l*, 4.6 Å average column stratum thickness; *t*, dendron tilt feature (48 ± 9°); *e*, 4.6 Å diffuse equatorial feature; *k*, 5.0 Å stacking distance along the column axis, correlation length is ∼94 Å (∼19 layers); *j*, (*hkl*) reflections of Φ_h^k phase.

includes L-Leu and L-Ile. (4) Dendritic dipeptides that, regardless of the thermal history of the sample, exhibit only a Φ_h^k phase. This is the case of the dendritic dipeptide containing L-Phe.

The role of the substituent of the second α-amino acid of the dipeptide on the thermal stability of its periodic array will be discussed by considering the dependence of the transition temperature from isotropic liquid to the Φ_h phase on the molar mass of the substituent. This dependence follows the trend Gly (1/98) > L-Ala (15/93) > L-Val (43/83) > L-Leu (57/79) > L-Ile (57/76) > L-Pro (42/69), where the ratio between parantheses refers to the molar mass of the substituent/transition temperature (in °C). In general, the transition temperature decreases as the molar mass of the substituent increases. There is a small temperature difference between L-Leu and L-Ile, although their substituents have equal molar mass but are constitutional isomers. L-Pro provides an inversion in this trend that is determined, as it will be discussed later, by the presence of a tertiary rather than a secondary amide in its structure. This decreases the number of the H-bonds from the inner part of the pore. While the above dependence would intuitively be expected, the dependence of the melting temperature of the Φ_h^k and Φ_x^k phases on the size of the substituent is, at least at first sight, unexpected. The following trend is observed in this case: L-Phe (91/121) > L-Leu (57/107) > L-Ile (57/104) > L-Val (43/100), where the ratio between parantheses is the same as that above. The higher the molar mass of the substituent, the higher the melting temperature of its corresponding periodic array. In addition, the dendritic dipeptides with low molar mass substit-

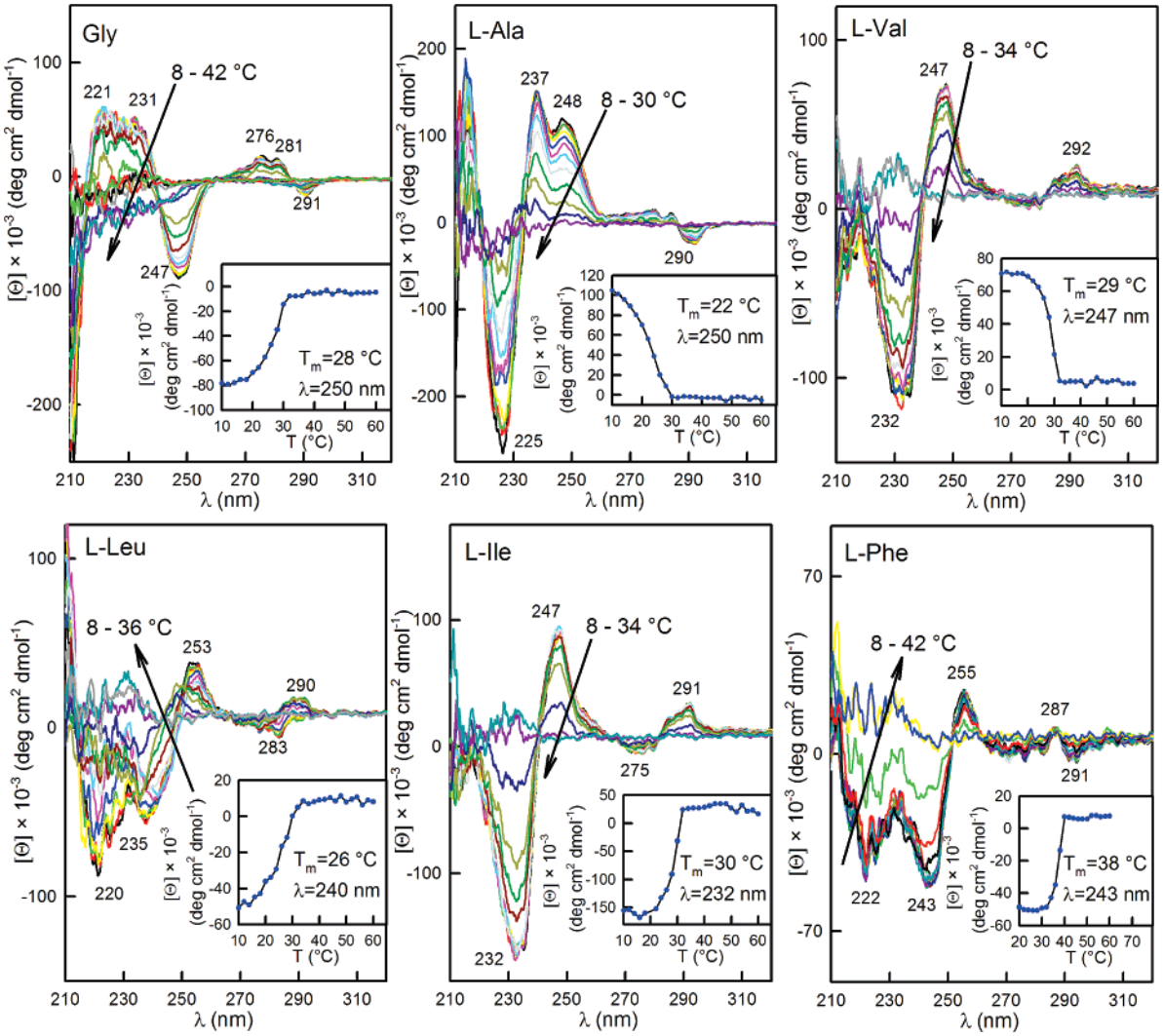

Figure 5. CD spectra (1.6×10^{-4} m in cyclohexane) of (4-3,4-3,5)12G2-CH_2-Boc-L-Tyr-X-OMe. The structure of the α-aminoacid X from the dipeptide and the temperature range are indicated. The insets illustrate the dependence of molecular ellipticity on temperature at a given wavelength. T_m is the middle point of the S shape dependence of the molecular ellipticity on temperature.

Table 2. Structural and Retrostructural Analysis of the Φ_h, $\Phi_h{}^k$, and Φ_{r-c} Lattices of (4-3,4-3,5)12G2-CH_2-Boc-L-Tyr-X-OMe

X	T (°C)	X	$d_{10}{}^a/A_{10}{}^c$ $d_{20}{}^b/A_{20}{}^c$ $d_{40}{}^b/A_{40}{}^c$	$d_{11}{}^a/A_{11}{}^c$ $d_{11}{}^b/A_{11}{}^c$ $d_{22}{}^b/A_{22}{}^c$	$d_{20}{}^a/A_{20}{}^c$ $d_{31}{}^b/A_{31}{}^c$ $d_{51}{}^b/A_{51}{}^c$	$d_{21}{}^a/A_{21}{}^c$ $d_{02}{}^b/A_{02}{}^c$ $d_{42}{}^b/A_{42}{}^c$	$a = D_{col}{}^d$ (Å)	D_{pore} (Å)	ρ^e (g/cm^3)	μ^f	t^g (Å)	α'^h (deg)
Gly	90	Φ_h	63.9/46.9	36.7/24.8	31.8/22.8	24.1/5.4	73.6 ± 0.4	11.7 ± 0.8	1.01	11.0	4.6	32.7
L-Val	70	Φ_h	67.8/40.3	38.9/28.0	34.0/28.4	25.7/3.3	78.3 ± 0.4	14.2 ± 1.2	1.03	11.4	4.6	31.6
	50	Φ_{r-c}	76.0/16.3	67.6/20.0	42.1/12.3	38.0/15.1	92.6 ± 0.6^i	15.3 ± 2.4^k				
			37.7/12.4	33.7/14.1	28.3/4.2	26.9/4.3	75.9 ± 0.5^j	12.5 ± 1.9^l				
L-Leu	85	$\Phi_h{}^k$	66.8/44.9	38.1/34.9	33.7/20.2	25.1/5.7	77.3 ± 0.4	10.1 ± 1.6	1.02	11.2	4.9	32.1
L -Ile	75	Φ_h	63.9/55.3	36.9/20.9	32.0/16.7		74.0 ± 0.4	12.4 ± 1.8	1.02	11.2	4.6	32.1
L -Phe	65	$\Phi_h{}^k$	55.0/46.4	31.8/27.8	27.9/17.8	20.2/8.0	63.5 ± 0.4	9.4 ± 0.8	1.11	9.1	5.0	39.6
L- Pro	25	Φ_h	70.4/39.8	40.7/26.1	35.4/26.4	26.8/7.7	81.4 ± 0.4	15.1 ± 1.6	1.0	11.8	4.6	30.5

[a,b] d-spacings of the Φ_h and Φ_{r-c} phase, respectively (in Å). [c] Peak amplitude scaled to the sum of the observed diffraction peaks (in arbitrary units). [d] Lattice parameter of Φ_h, $a = 2\langle d_{100}\rangle/\sqrt{3}$, $\langle d_{100}\rangle = (d_{100} + \sqrt{3}d_{110} + \sqrt{4}d_{200} + \sqrt{7}d_{210})/4$. [e] Experimental density at 22 °C. [f] Number of dendrons per column stratum $\mu = (\sqrt{3}N_A D^2 t\rho)/2M$, where $N_A = 6.0220455 \times 10^{23}$ mol^{-1} (Avogadro's number), M is the molecular weight of the dendrons, and [g] t is the average height of the column stratum, calculated from the XRD of the oriented fibers as features k or l from Figures 4 and 10. [h] $\alpha' = 2\pi/\mu$; D_{col} along the [i] long ***a*** and [j] short ***b*** axis, $D_{col}{}^{(along\ b)} = \boldsymbol{b} = 75.9$ Å, $D_{col}{}^{(along\ a)} = \epsilon D_{col}{}^{(along\ b)}$ where $\epsilon = 1.2 =$ is the fitted ellipticity ratio (see Supporting Information Figures SF7, SF8 and Table ST3); D_{pore} along the [k] ***a*** and [l] ***b*** axis.

uents do not crystallize or, as it will be discussed later, crystallize very slow. This trend is opposite to that observed for the transition from the isotropic to Φ_h phase. The hypothesis for the second trend is that large nonpolar substituents like those of L-Val, L-Leu, L-Ile mediate a higher rate of crystallization, most probably due to their hydrophobic character, while in the case of the aromatic substituent of L-Phe it is due to $\pi-\pi$ stacking. This hypothesis will be discussed in one of the next subchapters. In order to address the role of the substituent on crystallization, all dendritic dipeptides were annealed at various

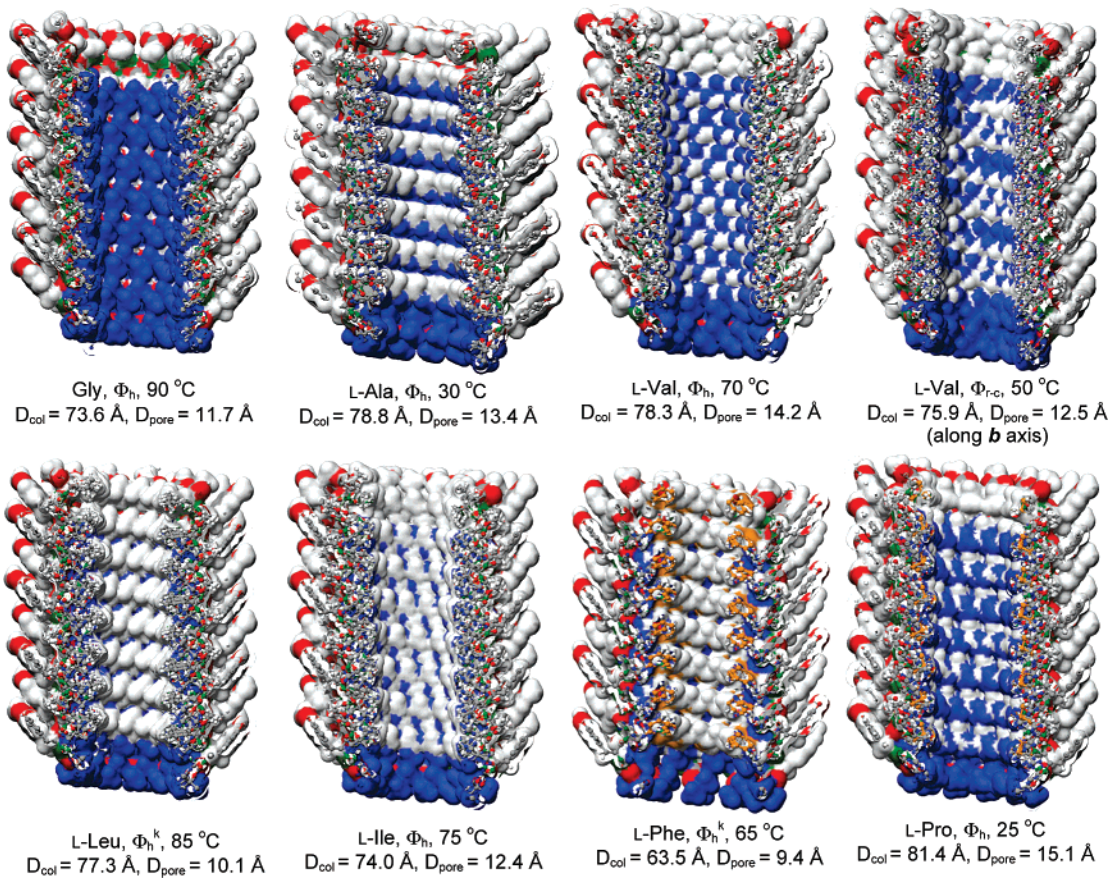

Figure 6. Cross sections of the molecular models of helical supramolecular pores assembled from (4-3,4-3,5)12G2-CH_2-Boc-L-Tyr-X-OMe constructed with the aid of XRD data from Table 2. The structure of α-aminoacid X from dipeptide, phases, temperatures, D_{col}, and D_{pore} are indicated. Color code: $-CH_3$ from the protective group of Tyr, blue; $-CH_3$ of the methylester of the second α-amino acid, white; C, gray; O, red; N−H, green.

temperatures, both in the Φ_h phase and in the isotropic liquid. Figure 2 illustrates the main results of these experiments. Only the dendritic dipeptides based on Gly and L-Pro do not crystallize. The dendritic dipeptides based on L-Ala, L-Val, L-Leu, L-Ile, and L-Phe form Φ_h^k and Φ_x^k phases, respectively. Details of their structural analysis will be presented in a different subchapter. The lowest rate of crystallization was observed in the case of dendritic dipeptide based on L-Ala, followed by L-Val, L-Ile, L-Leu, and L-Phe.

The powder small-angle XRD of all dendritic dipeptides recorded at the indicated temperature in Φ_h and Φ_h^k phases are shown in Figure 3. The enhanced amplitude of their (11), (20), and (21) peaks provides an indication for a porous column.[10,11] The diameter of the pore (D_{pore}) was calculated by the reconstruction of the XRD peak positions and intensities using the electron density of the dendritic dipeptide and considering a three-phase intracolumnar model consisting of regions of aliphatic, aromatic together with dipeptide, and a hollow center, by using the method reported previously (Figures SF7 and SF8).[10,11e] The column diameter (D_{col}) and D_{pore} calculated as mentioned above are summarized in Table 2 together with the XRD data used for their calculation and the experimental densities (ρ). It is interesting to observe that there is an unusual correlation between D_{pore} and the size of the second α-amino acid substituent. Gly that has H as the substituent provides a smaller D_{pore} than those of L-Val, L-Ile, and L-Pro that have larger substituents. L-Leu and L-Phe that have a methylene group between a phenyl and isopropyl group, respectively, have the lowest D_{pore}. An explanation of this trend will be provided in a different subchapter.

Structural Analysis of Oriented Fibers by Small- and Wide-Angle XRD. The combined small- and wide-angle XRD data recorded from the oriented fibers of (4-3,4-3,5)12G2-CH_2-Boc-L-Tyr-X-OMe with X = Gly, L-Val, L-Leu, L-Ile, L-Phe, and L-Pro together with the assignment of the diffraction peaks are shown in Figures 4, SF4, and SF6. The *X* shape of *i* diffraction indicates that the columns obtained from X = Gly, L-Val, L-Leu, L-Ile, and L-Pro exhibit a short-range helical structure. In the case of X = L-Phe the *i* diffraction is most probably overlapped by the intense *j* and *k* diffractions. The average thickness of the column stratum is determined from diffractions *l* and *k* and is summarized as value *t* in Table 2. The dendron tilt (*t*) is most visible in the case of L-Val. The helical structure of the supramolecular columns is also supported by circular dichroism (CD) experiments that will be discussed later for the case of X = Gly, L-Val, L-Leu, L-Ile, and L-Phe and compared with the CD experiments reported for L-Ala.[10]

Self-Assembly in Solution. A combination of 500 MHz ^{1}H NMR, CD, and UV spectroscopies was used to study the self-assembly in the solvophobic solvent cyclohexane.[10,11] Here we will discuss the analysis by CD (Figures 5, SF1 and SF2). The achiral dendritic alcohols (4-3,4-3,5)nG2-CH_2OH that are precursors to the dendritic dipeptides self-assemble into racemic helical columns.[11c] Therefore, the stereochemistry of the dipeptide only selects the twist sense of the racemic supramolecular

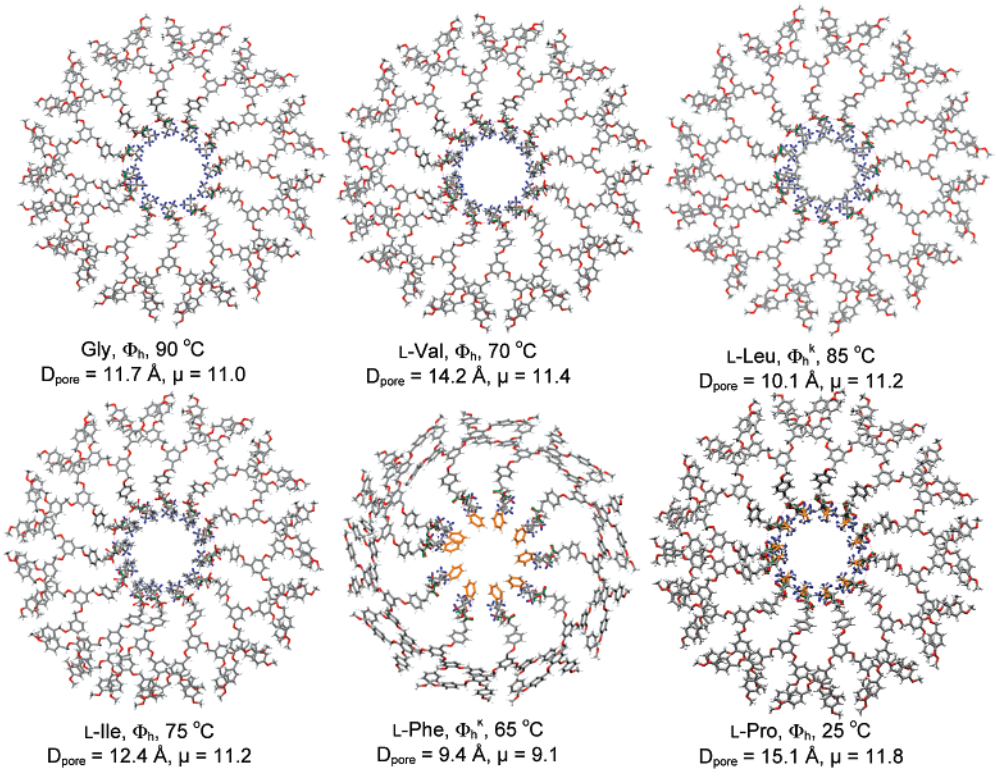

Figure 7. One layer of the top view of the helical supramolecular pores assembled from (4-3,4-3,5)12G2-CH_2-Boc-L-Tyr-X-OMe. The structure of α-aminoacid X from the dipeptide, the number of dendritic dipeptides (μ) forming the cross section, and D_{pore} are indicated. Color code: $-CH_3$ from the protective group of Tyr, blue; $-CH_3$ of the methylester of the second α-amino acid, white; C, gray; O, red; N−H, green.

helix.[10,11] Additional examples of racemic helical supramolecular dendrimers assembled from achiral dendrons are known.[16] This self-assembly process relates to examples in which a stereocenter selects the twist sense of a racemic helical structure[17] and agrees with the principles elaborated by Green,[18a] although the detailedmechanism is under elucidation.[18b,c] The assembly of the helical supramolecular structures in the solvophobic solvent cyclohexane was analyzed by CD (Figures 5, SF1, and SF2) and UV (Figures SF1 and SF2).[10,11]

For comparison, the CD of the dendritic dipeptide with X = L-Ala is also included in Figure 5. The molecular solutions of all dendritic dipeptides show a positive Cotton effect at 230 nm (Figures SF1 and SF2). On cooling, self-assembly takes place and Cotton effects associated with the aromatic part of the dendrons[10,11] are observed. The CD spectra of dendritic dipeptides based on X = L-Val and L-Ile exhibit similar Cotton effects, and their CD spectra are almost identical to that of (4-3,4-3,5)6G2-CH_2-Boc-L-Tyr-L-Ala-OMe.[11c] The CD of X = L-Leu resembles that of X = L-Phe. These two pairs of similar CD spectra show that related α-amino acid substituents (Scheme 1) induce similar conformations of the dendron in the supramolecular structure. The CD of X = Gly shows inversion of all Cotton effects with $\lambda < 260$ nm when compared to the CD of X = L-Leu. All these trends demonstrate the role of the substituent of X on the conformation of the dendron in the self-assembled structure and support the allosteric regulation mechanism[12] advanced previously.[11a−c] The similarity between the CD pairs L-Val, L-Ile and L-Leu, L-Phe correlates with that of their phase behavior in the solid state (Figure 1). The supramolecular structures with large hydrophobic substituents are also more stable in solution (see T_m in Figure 5). Gly provides an exception from this trend. This dependence is also in line with that observed in the solid state (Figure 1). L-Pro does not assemble into a helical structure in the range of temperature investigated in Figure 5. This is also expected, since it displays a much less stable structure in the solid state (Figure 1), and therefore, in solution the helical structure must form at lower temperatures.

Structural and Retrostructural Analysis of the Supramolecular Pores. In addition to D_{col} and D_{pore} calculated from small-angle XRD experiments, Table 2 summarizes the number of dendrons (μ) forming a column cross section of average height (t) determined from wide-angle XRDs on oriented fibers (l and k in Figures 4, SF4, and SF6) and the experimental densities (ρ).[10,11,15,16e] These data were used to generate the molecular models shown in Figure 6.[10,11] These models dem-

(16) (a) Kwon, Y. K.; Chvalun, S.; Schneider, A.-I.; Blackwell, J.; Percec, V.; Heck, J. A. *Macromolecules* **1994**, *27*, 6129−6132. (b) Kwon, Y. K.; Chvalun, S. N.; Blackwell, J.; Percec, V.; Heck, J. A. *Macromolecules* **1995**, *28*, 1552−1558. (c) Percec, V.; Glodde, M.; Bera, T. K.; Miura, Y.; Shiyanovskaya, I.; Singer, K. D.; Balagurusamy, V. S. K.; Heiney, P. A.; Schnell, I.; Rapp, A.; Spiess, H.-W.; Hudson, S. D.; Duan, H. *Nature* **2002**, *419*, 384−387. (d) Percec, V.; Glodde, M.; Peterca, M.; Rapp, A.; Schnell, I.; Spiess, H. W.; Bera, T. K.; Miura, Y.; Balagurusamy, V. S. K.; Aqad, E.; Heiney, P. A. *Chem.−Eur. J.* **2006**, *12*, 6298−6314. (e) Percec, V.; Peterca, M.; Sienkowska, M. J.; Ilies, M. A.; Aqad, E.; Smidrkal, J.; Heiney, P. A. *J. Am. Chem. Soc.* **2006**, *128*, 3324−3334.
(17) (a) Hill, D. J.; Mio, M. J.; Prince, R. B.; Hughes, T. S.; Moore, J. S. *Chem. Rev.* **2001**, *101*, 3893−4012. (b) Brunsveld, L.; Zhang, H.; Glasbeek, M.; Vekemans, J. A. J. M.; Meijer, E. W. *J. Am. Chem. Soc.* **2000**, *122*, 6175−6182. (c) Percec, V.; Rudick, J. G.; Peterca, M.; Wagner, M.; Obata, M.; Mitchell, C. M.; Cho, W.-D.; Balagurusamy, V. S. K.; Heiney, P. A. *J. Am. Chem. Soc.* **2005**, *127*, 15257−15264. (d) Jin, W. I.; Fukushima, T.; Niki, M.; Kosaka, A. I.; Ishii, N. I.; Aida, T. *Proc. Natl. Acad. Sci. U.S.A.* **2005**, *102*, 10801−10806.
(18) (a) Green, M. M.; Park, J.-W.; Sato, T. I.; Teramoto, A. I.; Lifson, S.; Selinger, R. L. B.; Selinger, J. V. *Angew. Chem., Int. Ed.* **1999**, *38*, 3139−3154. (b) Jonkheijm, P.; van der Schoot, P.; Schenning, A. P. H. J.; Meijer, E. W. *Science* **2006**, *313*, 80−83. (c) Percec, V.; Ungar, G.; Peterca, M. *Science* **2006**, *313*, 55−56.

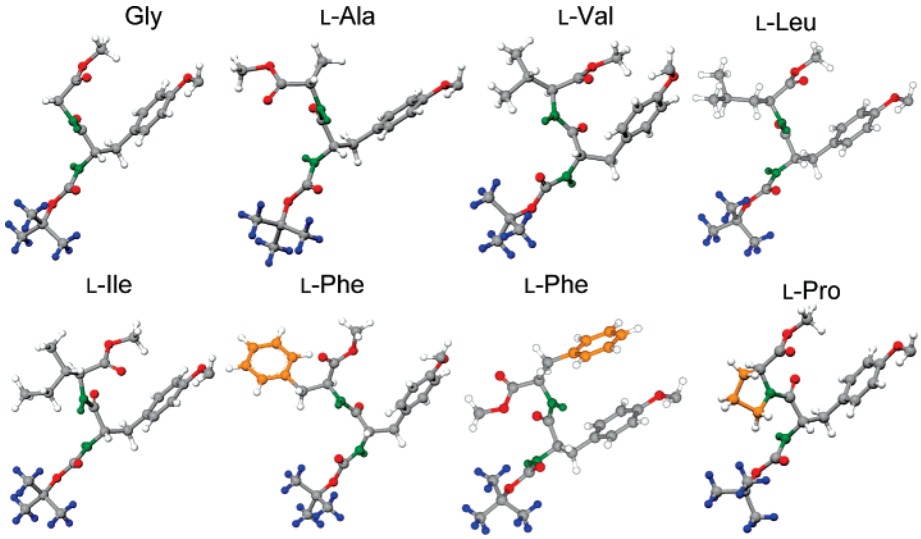

Figure 8. Conformation of the dipeptides in the helical supramolecular pores assembled from (4-3,4-3,5)12G2-CH_2-Boc-L-Tyr-X-OMe (data from Figures 6 and 7; L-Val in Φ_h phase). The structure of α-aminoacid X from dipeptide and the structure of the dendritic dipeptides are indicated. Color code: $-CH_3$ from the protective group of Tyr, blue; $-CH_3$ of the methylester of the second α-amino acid, white; C, gray; O, red; N−H, green.

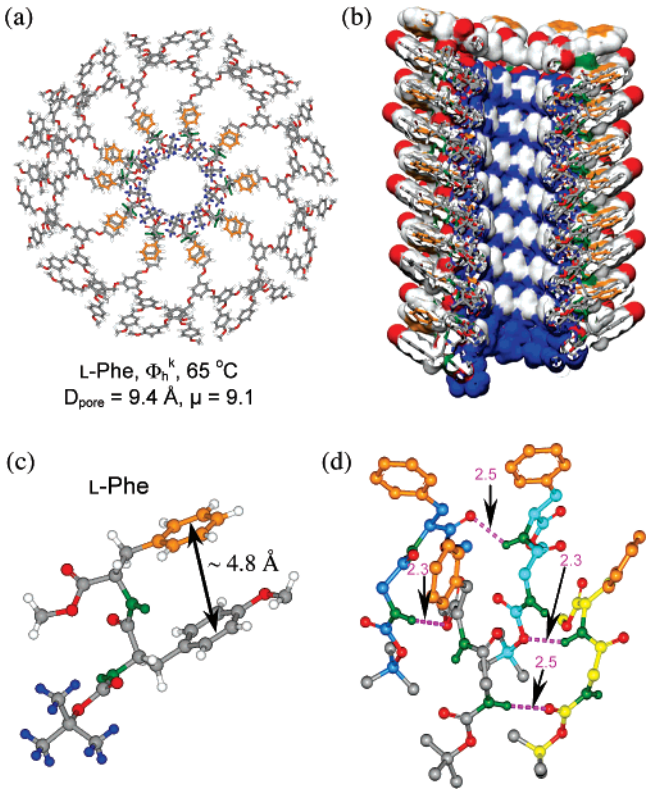

Figure 9. Alternative conformation of the dendritic dipeptide in the helical supramolecular pores assembled from (4-3,4-3,5)12G2-CH_2-Boc-L-Tyr-L-Phe-OMe: one column stratum top view (a), pore cross section (b), detail of the dipeptide conformation (c), and detail of the H-bonding network (length in Å) (d).

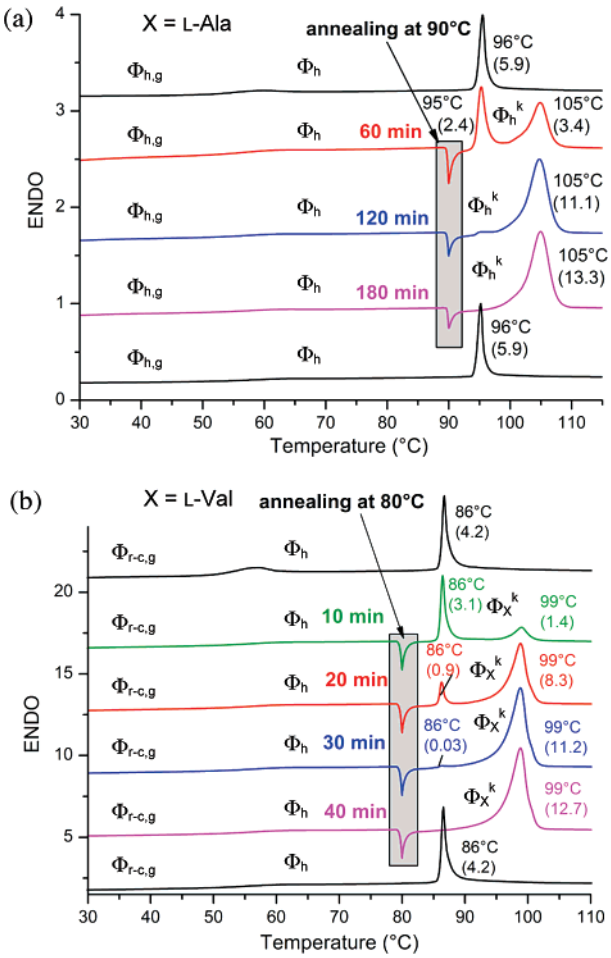

Figure 10. Heating DSC traces of (4-3,4-3,5)12G2-CH_2-Boc-L-Tyr-X-OMe with (a) X = L-Ala and (b) X = L-Val. Both in (a) and (b) the top DSC traces represent second heating scans of the as-prepared samples, while the subsequent DSC traces illustrate heating scans after the sample was annealed at the mentioned temperature, for the indicated time; the bottom DSC traces show heating scans after the final annealed sample was cooled from the isotropic state.

onstrate that larger hydrophobic substituents cover the inner part of the pore more efficiently than Gly. Most probably this is responsible for their contribution to the stabilization of the 3-D structure and the enhanced tendency toward crystallization.

Extremely interesting is the case of L-Phe that, according to this model, generates a helical $\pi-\pi$ stack of phenyl groups located in the inner part of the pore. The top views of a single layer of these supramolecular columns from Figure 6 are shown in Figures 7 and SF11. The conformation of the individual dipeptides from the supramolecular structures from Figure 6 are illustrated in Figure 8 together with an alternative model

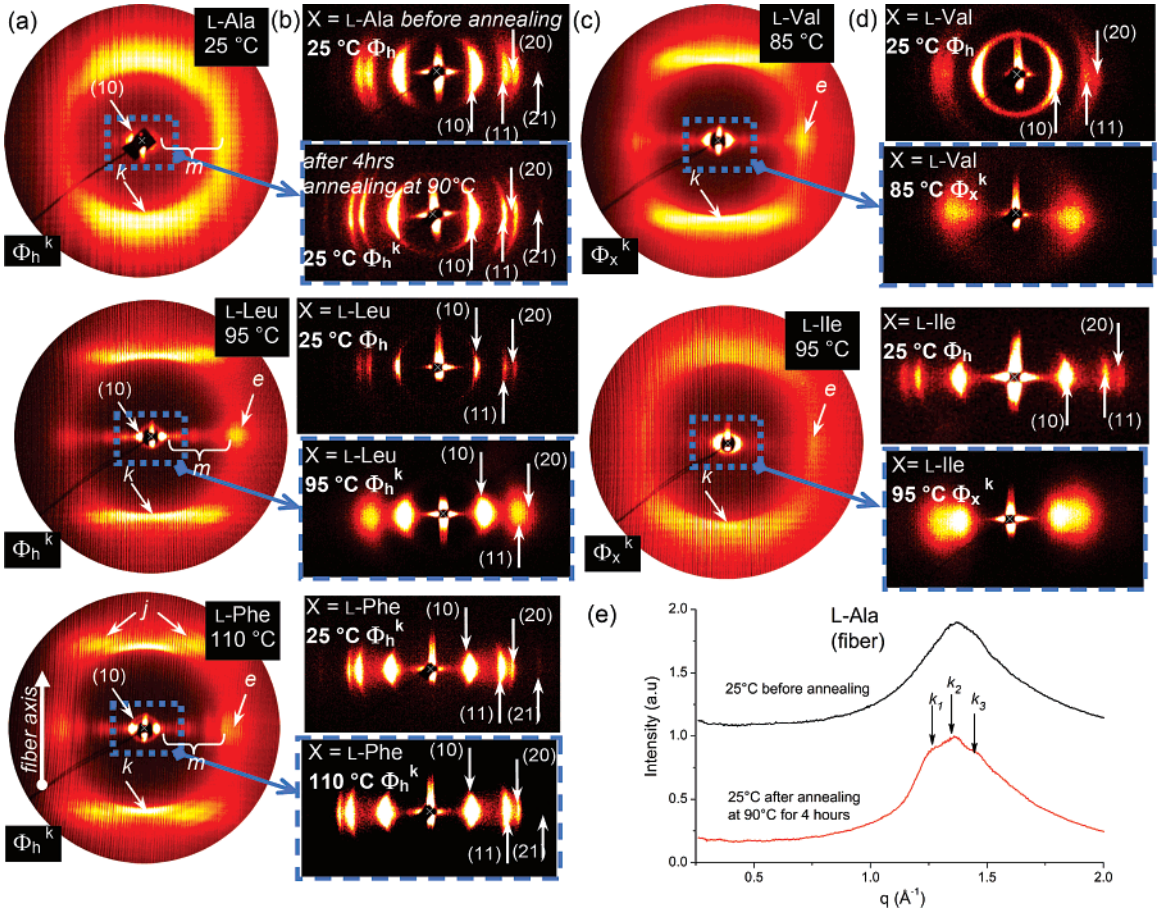

Figure 11. Combined small- and wide-angle XRD patterns of oriented fibers of (4-3,4-3,5)12G2-CH_2-Boc-L-Tyr-X-OMe obtained after annealing at the indicated temperatures for 1 h or as marked (columns a and c). The structure of α-amino acid X from dipeptide is indicated. The phase notations are as those in Figure 1. Small-angle XRD patterns of the same oriented fibers collected before and after annealing at the indicated temperatures for 1 h or as marked (columns b and d). Meridional q-plots for X = L-Ala demonstrating crystallization during annealing as indicated by the k_1, k_2, k_3 sharp peaks (e). In all structures k = 5.0 Å represents stacking registry along the column axis; *e*, diffuse equatorial feature; (10), (11), (20), (21), (*hk*0) reflections of the Φ_h phase; *j*, (*hkl*) reflections of Φ_h^k phase; *m*, higher order (*hk*0) reflections of the Φ_h phase. For X = L-Val the correlation length of the wide angle meridional *k* feature (~80 Å) has the same order as the Φ_X^k lattice diffraction peak (~76 Å at 85 °C) calculated from the shown small angle pattern.

for the case of L-Phe. In all cases, except for L-Phe where two models are possible, the substituent of the α-amino acid is in the inner part of the pore, and this explains its contribution to the pore structure and stability. The dependence of D_{pore} on μ and on the projection of the solid angle of the dendron (α′) suggests, as observed previously,[11b,c] that as α′ decreases, μ and D_{pore} increase. Two conformers are shown in Figure 8 for L-Phe. The left one is for the model from Figures 6 and 7. The right one is for the model from Figure 9 in which the phenyl of L-Phe forms a $\pi-\pi$ stack with the phenyloxy group of L-Tyr in the outer part of the pore. This model is favored since it facilitates aromatic−aromatic rather than aromatic−aliphatic interactions. This model also explains the lower D_{col} self-assembled from this dendritic dipeptide (Table 2). Additional support for this model and elaboration of novel functional architectural motifs based on it will be reported.

Crystalline Supramolecular Pores and Their Impact on Pore Stability. In previous experiments the supramolecular pores forming Φ_h phases were stable below their glass transition temperature (T_g).[11a,b] Due to molecular motion in the Φ_h phase, above T_g, D_{pore} is temperature dependent. However, supramolecular pores forming Φ_h phases with intracolumnar order (Φ_h^{io}) are stable up to the isotropization temperature.[11b] Crystalline phases with hexagonal symmetry are expected to provide porous structures stable up to their melting temperature. Therefore, the crystallization of all dendritic dipeptides was investigated in Φ_h and in isotropic melt (Figures SF9, SF10, SF12−SF14). Figure 10 shows the annealing of X = L-Ala and L-Val in their Φ_h phase and the analysis of the crystallization process by DSC. The dendritic dipeptide with X = L-Ala requires 3 h of annealing at 95 °C for complete transformation of the Φ_h phase into Φ_h^k (Figures 10 and 11). Shorter annealing time produces a biphasic mixture containing Φ_h and Φ_h^k phases. However, the columnar hexagonal symmetry is maintained in the crystal state. The same annealing process for the case of X = L-Val induces a complete crystallization after 40 min at 80 °C. However, the crystal phase maintains a columnar structure (Φ_x^k) that was not yet elucidated (Figures 10 and 11).

The same Φ_x^k phase was obtained in the case of X = L-Ile (Figure 10). L-Phe and L-Leu crystallize in a Φ_h^k phase. This crystallization process can be induced also by annealing in the isotropic liquid (Figure SF 14). However, the crystal phase is less ordered when crystallization is induced in the isotropic melt. Regardless of the annealing temperature, the dendritic dipeptides based on Gly and L-Pro do not crystallize.

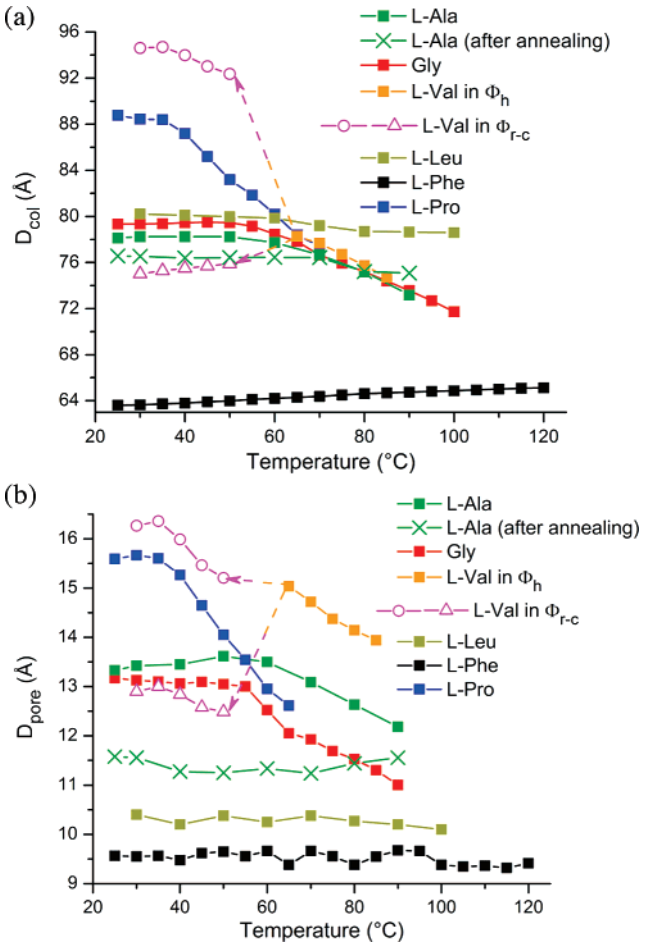

Figure 12. Dependence of (a) D_{col} and (b) D_{pore} on the temperature for the helical porous columns assembled from (4-3,4-3,5)12G2-CH_2-Boc-L-Tyr-X-OMe. The structure of X is indicated. For X = L-Val below 50 °C, the D_{col} and D_{pore} of the Φ_{r-c} phase are shown as calculated along the long ***a*** (circles) and short ***b*** (triangles) axis of the Φ_{r-c}, respectively. For X = L-Ala the annealing was done in the Φ_h phase at 90 °C for 4 h.

The dependence of D_{col} and D_{pore} on temperature was investigated both before and after crystallization for the case of L-Ala, in the Φ_h and Φ_{r-c} phases for L-Val, in the $\Phi_h{}^k$ phases for L-Phe and L-Leu, and in the Φ_h phase for the case of Gly and L-Pro (Figures 12, SF9, and SF10).

In the Φ_h phase D_{pore} is not dependent on temperature up to T_g, while in the $\Phi_h{}^k$ phase D_{pore} is stable up to the melting temperature. In the 2-D Φ_h phase the stability of D_{pore} is determined by the intracolumnar order that includes the network of H-bonds of the interdigitated dipeptides.[10,11] In the current case the substituent of X influences the number of the inter-peptide H-bonds and provides additional and complementary intermolecular interactions such as hydrophobicity in the case of alkyl substituents and $\pi-\pi$ stacking in the case of aryl substituents.

The H-bonding structures for two pairs of interdigitated peptides[10,11] are shown in Figure 13 for the case of X = Gly, L-Val, L-Leu, L-Ile, L-Phe, and L-Pro. In the case of X = Gly, L-Val, L-Leu, and L-Ile there are four in-layer and five interlayer H-bonds. In the case of L-Pro the tertiary peptide facilitates only two in-layer and two interlayer H-bonds. In addition, the bulky and conformationally restricted cyclic substituent of L-Pro explains the low thermal stability of its supramolecular pore since the reduced number of H-bonds is not counterbalanced

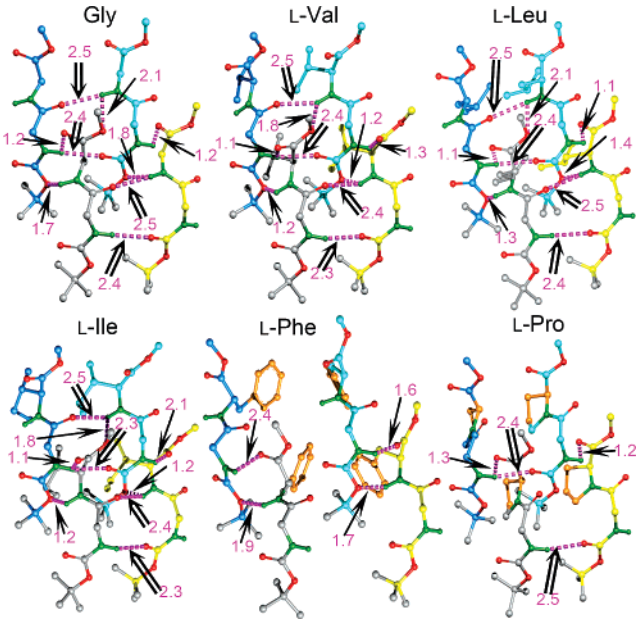

Figure 13. In-layer (double arrows) and interlayer (single arrows) H-bonding networks of the (4-3,4-3,5)12G2-CH_2-Boc-L-Tyr-X-OMe. The structure of X and H-bonding lengths (Å) are indicated. Four dipeptides from two interdigitated layers of the channel are shown. For simplicity, only the H-bonded hydrogen atoms are shown; the 4-phenyloxy group of L-Tyr is not shown. Color code: O, red; NH, green; each of the four dipeptides has its C atoms colored differently. For the case of X = L-Phe the model is from Figures 6, 7.

by other intermolecular interactions. The bulky substituent of L-Phe eliminates four interlayer and one in-layer H-bonds. However, by contrast with the case of L-Pro, in the L-Phe case the $\pi-\pi$ interactions created by its phenyl substituent overcome the reduced number of H-bonds and even enhance the tendency toward crystallization. The large and flexible alkyl substituents also facilitate the crystallization process. These trends will be exploited in the design of novel artificial α-amino acids that are expected to provide even more powerful pore stabilization strategies and new bioinspired pore functions.

Conclusions

The synthesis of dendritic dipeptides (4-3,4-3,5)12G2-CH_2-Boc-L-Tyr-X-OMe where X = Gly, L-Val, L-Leu, L-Ile, L-Phe, and L-Pro and their self-assembly in solution and in bulk are reported. The structural and retrostructural analysis of the supramolecular helical pores self-assembled from these dendritic dipeptides was compared with that of the reinvestigated dendritic dipeptide with X = L-Ala that was reported previously.[10,11a−c] All dendritic dipeptides were shown to self-assemble into helical pores that self-organize for the case of Gly and L-Pro into 2-D Φ_h and Φ_{r-c} lattices, for the case of L-Ala, L-Leu, and L-Phe into 2-D Φ_h and 3-D $\Phi_h{}^k$ lattices, and for the case of L-Val and L-Ile into 2-D Φ_h and Φ_{r-c} and in 3-D $\Phi_x{}^k$ lattices. These dendritic dipeptides provide the first examples of supramolecular helical pores that self-organize into crystal lattices. This result is important both for practical applications and for access to a more detailed structural analysis by XRD. In 2-D lattices, D_{pore} is stable only up to the glass transition temperature while, in 3-D crystals, it is stable up to the melting point. Unexpectedly, the smaller substituents of X provide more stable 2-D arrays, while the larger substituents facilitate crystallization via a hydrophobic process in the case of aliphatic substituents and

respectively via $\pi-\pi$ interactions in the case of aromatic substituents. Larger substituents provide higher melting temperatures of crystal phases, while smaller substituents provide higher isotropization temperatures of columnar liquid crystal phases. This study complements the previous investigations on the role of dipeptide stereochemistry,[11a] protective groups,[11b] dendron architecture and its alkyl groups[11c−e] and provides the molecular principles required to design new biologically inspired functions[10] with the aid of artificial nonpolar α-amino acids. Since these supramolecular helical pores represent dendronized supramolecular polymers, it is expected that this concept can be extended to self-organizable dendronized covalent polymers[17c,19] and, therefore, expand the scope and limitations of self-assembling dendrons in the design of complex functional matter.[20]

Acknowledgment. Financial support by the National Science Foundation (DMR-0548559 and DMR-0520020) and P. Roy Vagelos Chair at Penn, and discussions with Professor G. Ungar of Sheffield University, U.K. are gratefully acknowledged.

Supporting Information Available: Experimental section containing materials, techniques, and synthesis with structural and retrostructural analysis. This material is available free of charge via the Internet at http://pubs.acs.org.

JA071088K

(19) (a) Percec, V.; Ahn, C.-H.; Ungar, G.; Yeardley, D. J. P.; Möller, M.; Sheiko, S. S. *Nature* **1998**, *391*, 161−164. (b) Percec, V.; Ahn, C.-H.; Cho, W.-D.; Jamieson, A. M.; Kim, J.; Leman, T.; Schmidt, M.; Gerle, M.; Möller, M.; Prokhorova, S. A.; Sheiko, S. S.; Cheng, S. Z. D.; Zhang, A.; Ungar, G.; Yeardley, D. J. P. *J. Am. Chem. Soc*. **1998**, *120*, 8619−8613.

(20) (a) Emrick, T.; Fréchet, J. M. J. *Curr. Opin. Colloid Interface Sci*. **1999**, *4*, 15−23. (b) Tomalia, D. A. *Mater. Today* **2005**, *8*, 34−46. (c) Hecht, S. *Mater. Today* **2005**, *8*, 48−55. (d) Lehn, J.-M. *Proc. Natl. Acad. Sci. U.S.A.* **2002**, *99*, 4763−4768.